RSC Advances

PAPER

View Article Online
View Journal | View Issue

Cite this: *RSC Adv.*, 2026, **16**, 24621

Metal anchoring strategy: electrochemical sensor with excellent performance in gastrointestinal secretions

Juanjuan Ji, *[a] Baohong Shen,[b] Fang Yang,[a] Sujuan Li,[c] Yuyu Wang,[a] Lu Yang[a] and Hao Lin[d]

Received 20th February 2026
Accepted 27th April 2026

DOI: 10.1039/d6ra01510g

rsc.li/rsc-advances

In order to monitor the health level of the digestive tract, especially to achieve real-time monitoring of 3,4-dihydroxyphenylalanine (DA) and uric acid (UA) levels in saliva. This work proposes a strategy for *in situ* adsorption of Au^{3+} ions in HKUST-1 pore and *in situ* reduction to Au^0, anchoring in HKUST-1 pores. Au@HKUST-1 maintaining stability in complex environments lays the foundation for its application in gastrointestinal monitoring. The sensor was successfully prepared by Au@HKUST-1 which can achieve real-time monitoring of DA and UA. The excellent monitoring performance is attributed to the strong interaction between Au^0 and HKUST-1, which enables Au@HKUST-1/GCE to exhibit excellent monitoring performance for DA, UA and mixtures, with detection limits of 0.06, 0.38, 0.10, and 0.15 μM, respectively. In artificial saliva, Au@HKUST-1/GCE has demonstrated excellent recovery rates, providing feasible strategies for monitoring and timely intervention in gastrointestinal diseases.

1 Introduction

The digestive system is composed of multiple organs that are essential for nutrient absorption and metabolic regulation, playing a crucial role in maintaining normal physiological functions and supporting the proper operation of the immune system.[1–3] The human digestive system comprises the digestive tract, including the oral cavity, esophagus, stomach, and intestines, as well as digestive glands such as the pancreas and kidneys.[4] After food enters the oral cavity, it is transported through the esophagus and stomach into the intestines, where digestion is facilitated by secretions from the digestive glands.[5] Ultimately, undigested and unabsorbed residues are excreted from the body through the colorectal tract in the form of feces.[6] As the first line of defense and a fundamental protective barrier of the digestive system, maintaining the homeostasis of the gastrointestinal tract is of paramount importance. However, dietary intake and pathological conditions can induce alterations in biochemical indicators within the digestive tract, thereby leading to changes in physiological activities and overall health status.[7–10] Consequently, monitoring physiologically active substances in the digestive tract is of great significance for assessing gastrointestinal functional states and guiding timely intervention to prevent sub-health conditions.[11–15]

Saliva, as one of the most important secretions of the digestive system, contains dozens of biomarkers that can be exploited for health management and clinical diagnosis[16–21] Conventionally, the concentrations of target analytes in saliva can be evaluated using traditional analytical instruments. However, these approaches generally require complicated sample pretreatment procedures and expensive, bulky equipment. In comparison, electrochemical sensing has emerged as a promising analytical technique owing to its facile fabrication, rapid response, and high sensitivity. Although various functional materials have been engineered as electrochemical sensors for the detection of specific analytes, their sensing performance remains largely constrained by the probe materials immobilized on the working electrode. Therefore, it is highly desirable to develop robust sensing materials that can maintain structural and functional stability in the gastrointestinal environment for digestive system health monitoring. Metal–organic frameworks (MOFs),[22–24] which due to featuring large specific surface areas, tunable pore architectures, and highly ordered structures, have demonstrated remarkable potential in the design of sensing probes. If MOFs can be modified through simple and effective strategies to enable reliable sensing in gastrointestinal environments, such materials would substantially expand the application scope of MOF-based sensors in digestive health monitoring.

3,4-Dihydroxyphenylalanine (DA)[25,26] and uric acid (UA)[27–29] are of particular interest due to their close association with

[a]*Department of Gastroenterology, The First Affiliated Hospital of Xinxiang Medical University, Henan 453100, China. E-mail: juanjuanSCI@126.com*

[b]*Department of Oral and Maxillofacial Surgery, The First Affiliated Hospital of Xinxiang Medical University, Henan 453100, China*

[c]*Department of Integrated Traditional Chinese and Western Medicine, The First Affiliated Hospital of Xinxiang Medical University, Henan 453100, China*

[d]*Jiangsu Haicheng Pharmaceutical Materials Co., Ltd, Taizhou, Jiangsu 225300, China*

neurological and metabolic disorders. Typically, hyperuricemia[30] often stemming from renal complications due to impaired purine metabolism can severely impact normal daily activities with advancing age. The concentration level of DA within the body significantly influences the heightened likelihood of developing neurodegenerative diseases.[31,32] Continuous monitoring of DA and UA is therefore essential for disease management, especially in elderly populations. Consequently, monitoring these compounds aids in enhancing health management. Current commercial sensors for DA and UA monitoring necessitate invasive sampling procedures, which not only expose patients to infectious disease risks but also hinder real-time health monitoring. Given the ease of collection and correlation with plasma levels, research into gastrointestinal secretion sensors is crucial for providing real-time feedback monitoring and treatment guidance for neurological and renal disorders.

This work proposed a method for preparing a sensor for detecting gastrointestinal secretions based on HKUST-1. Au^{3+} ions were adsorbed into HKUST-1 through weak intermolecular interactions, and then the reduced Au^0 is anchored in the pore structure of HKUST-1 through the introduction of a reducing agent. A modified glassy carbon electrode by Au@HKUST-1 was used to successfully prepare an electrochemical sensor for simultaneous monitoring of DA and UA in saliva. Due to the strong interaction between Au^0 and HKUST-1, the sensor exhibits excellent response performance and low detection limit. It is worth noting that this sensor exhibits excellent anti-interference performance. The successful preparation of this sensor not only provides new ideas for saliva detection, but also serves as a reference for gastrointestinal monitoring and health guidelines.

2 Materials and methods

2.1 General information

All reagents and solvents were obtained from commercial sources and used without further purification. Fourier transform infrared (FT-IR) spectra (KBr pellets) were recorded in the range 4000–400 cm^{-1} on Nicolet 6700 using the KBr pellet method. The electrochemical tests were conducted on a CHI-660E electrochemical workstation.

2.2 Synthesis of HKUST-1

870 mg $Cu(NO_3)_2$ was distributed in 10 mL water. Subsequently, 10 mL of methanol and 1 mL DMF solution containing 220 mg H_3BTC was poured into the above solution and the reaction was stirred continuously for 24 h at 80 °C. The blue crystal was collected by centrifugation, washed three times with fresh methanol, and dried at 60° over night.

2.3 Synthesis of Au@HKUST-1

Methanol (10 mL) was added to a clean beaker, followed by 50 mg of HKUST-1. The beaker was then placed in an ultrasonic machine for 10 min. A magnetic stir bar was added, and the beaker was placed on a magnetic stirrer under magnetic stirring for 10 min at room temperature to ensure the uniform dispersion of HKUST-1 in the methanol solution. Separately, 0.2 mL of 0.1 mol L^{-1} $HAuCl_4$ solution were slowly dripped into the stirring HKUST-1 solution. Stirring was continued on a magnetic stirrer at room temperature for 10 min to ensure the complete dispersion of $HAuCl_4$ in the methanol solution. 10 mL of methanol was added to another clean beaker, followed by the addition of 30 mg of $NaBH_4$. The beaker was placed in an ultrasonic machine for 10 min to ensure complete dissolution of $NaBH_4$ in the methanol solution. While stirring HKUST-1 solution at a speed of 500 rpm, $NaBH_4$ solution was slowly added, and stirring was continued for 2 h at room temperature. The resulting mixture was then centrifuged five times with deionised water and methanol to remove all impurities except Au@HKUST-1, leaving only pure Au@HKUST-1.

2.4 Electrochemical experiments

A bare glass carbon electrode (GCE) with a radius of 3 mm was polished continuously on a chamois for 60 s and then rinsed with deionised water. A total of 1 mg of samples, 200 μL ethanol, and 100 μL of Nafion solution (5 wt%) were first dispersed in 200 μL of water to produce a suspension. Following a 30 minutes sonication-assisted treatment, the homogeneous sample suspensions were loaded onto GCE. The electrochemical tests were conducted on a CHI-660E electrochemical workstation with a three-electrode configuration. An Ag/AgCl (saturated KCl) electrode and a Pt were used as a reference electrode and counter-electrode, respectively; GCE loaded with samples were used as working electrodes. If no otherwise specified, the error bars represent the standard deviations of three independent measurements.

2.5 LOD calculation

The LOD was calculated by,

$$\mathrm{LOD} = 3S/K$$

where S is the blank multiple measurement standard deviation, K is the calibration curve slope.

3 Results and discussion

3.1 Characterization of the synthesized

The synthesis of the Au@HKUST-1 was carried out *via* a stepwise strategy. First, HKUST-1 with a microporous structure was synthesized through a solvothermal coordination reaction between the organic ligand benzene-1,3,5-tricarboxylic acid (BTC) and Cu(II) metal nodes, with the synthetic protocol optimized based on previous reports (Fig. 1a).[33] The powder X-ray diffraction (PXRD) pattern of the as-synthesized HKUST-1 shows excellent agreement with the simulated PXRD pattern calculated from its single-crystal structure, confirming the high phase purity and crystallinity of the framework (Fig. S1). As expected, the face-centered cubic network constructed from dioper paddlewheel units and BTC ligands features intrinsic pore channels with pore sizes of 9.0 Å and 3.5 Å, which are

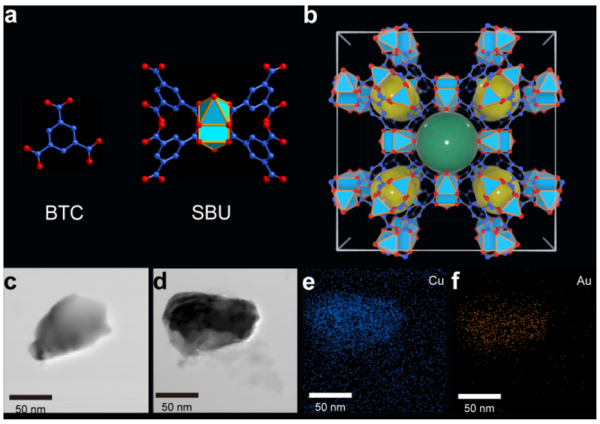

Fig. 1 (a) Organic ligands and metal nodes, (b) schematic diagram of HKUST-1 stacking structure and pore channels, (c) TEM image of HKUST-1, (d) TEM image of Au@HKUST-1, (e) and (f) the corresponding elemental mapping of Au@HKUST-1.

sufficiently large to accommodate and stabilize relatively bulky guest molecules (Fig. 1b).

Subsequently, the as-prepared HKUST-1 was subjected to solvent exchange to expose the pore channels initially occupied by solvent molecules or coordinatively unsaturated metal sites. The activated HKUST-1 was then thoroughly mixed with $HAuCl_4$, followed by the addition of a reducing agent under continuous stirring. During this process, Au^{3+} ions adsorbed within the pores of HKUST-1 were reduced to Au^0 and confined inside the framework cavities, accompanied by a distinct color change of the crystals from blue to dark blue–black. The crystalline phase of Au@HKUST-1 was further examined by PXRD to verify the successful formation of the composite material. As shown in Fig. 2c and S2, the diffraction peaks of Au@HKUST-1 closely match those of pristine HKUST-1, with only negligible

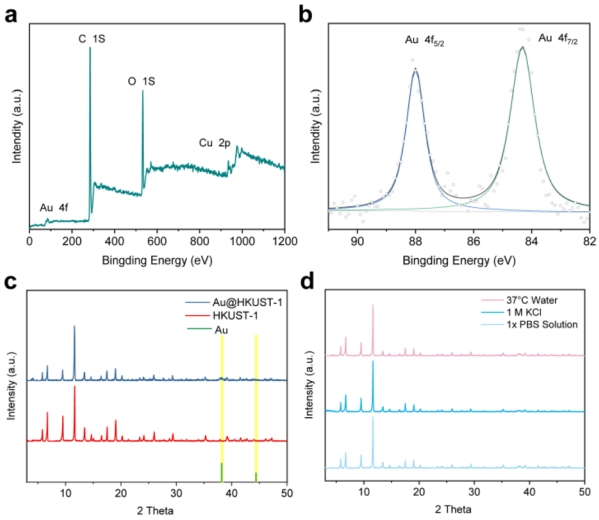

Fig. 2 (a) XPS spectrum of Au@HKUST-1, (b) the high-resolution Au 4f XPS spectrum of Au@HKUST-1, (c) XRD patterns of HKUST-1, Au@HKUST-1 and Au, (d) the chemical stability of Au@HKUST-1.

differences in peak intensity. This observation indicates that the introduction of Au into the open porous framework does not induce structural collapse. Notably, weak diffraction peaks appearing at approximately 38.2°and 44.4° can be assigned to the (111) and (200) crystal planes of metallic Au^0, respectively, confirming the presence of Au^0 in the composite. The relatively low intensity of these peaks can be attributed to the small size of the formed gold nanoparticles. In addition, a slight leftward shift of the diffraction peaks of Au@HKUST-1 compared with those of HKUST-1 was observed, which is ascribed to subtle lattice expansion induced by the incorporation of Au^0. Fourier transform infrared (FT-IR) spectra of HKUST-1 and Au@HKUST-1 further confirm that the introduction of Au^0 does not alter the chemical structure of the parent framework (Fig. S3).

X-ray photoelectron spectroscopy (XPS) was employed to investigate the chemical composition and electronic states of the Au^0 loaded composite. As shown in Fig. 2a, the survey XPS spectrum of Au@HKUST-1 clearly displays characteristic signals corresponding to Cu, C, O, and Au elements. In particular, the presence of distinct Au related peaks provides compelling evidence for the successful incorporation of gold. The high-resolution Au 4f spectrum further reveals the chemical state of Au in the composite with an atomic ratio of 0.18% of total elemental content. As illustrated in Fig. 2b, the binding energies located at 84.3 eV and 88.0 eV are assigned to the Au $4f_{7/2}$ and Au $4f_{5/2}$ orbitals, respectively. The energy separation of 3.7 eV between these two peaks is characteristic of metallic Au^0, indicating that Au exists predominantly in the zero-valent state in Au@HKUST-1. Combined with the PXRD results, these findings confirm the successful synthesis of the Au@HKUST-1 composite and validate the feasibility of the adopted synthetic strategy.

The microstructures of HKUST-1 and Au@HKUST-1 were further characterized by transmission electron microscopy (TEM). As shown in Fig. 1, TEM images of HKUST-1 and Au@HKUST-1, respectively, revealing that the overall morphology of the framework remains largely unchanged after Au loading. Notably, ultrafine Au^0 nanoparticles are observed to be uniformly distributed on the surface of HKUST-1. The corresponding energy-dispersive X-ray spectroscopy (EDS) elemental mapping (Fig. 1f) clearly demonstrates the homogeneous distribution of Au throughout the composite, further confirming the successful *in situ* formation of Au@HKUST-1.

3.2 Chemical stability

Considering the complexity and variability of the gastrointestinal environment, the chemical stability of Au@HKUST-1 under simulated digestive conditions was systematically evaluated. To comprehensively assess its stability, the composite was directly immersed in a series of challenging environments, including pure water at 37 °C, saline solution, and buffered solutions (1 M KCl and 1× PBS). FT-IR spectra recorded after immersion show no significant changes in characteristic absorption bands, indicating that the chemical structure of Au@HKUST-1 remains intact under these conditions.

Consistently, the PXRD patterns exhibit no noticeable variations in diffraction peak positions or intensities, suggesting that Au^0 is firmly anchored within the framework pores without leaching or framework degradation (Fig. 2d and S4). These results collectively demonstrate the high chemical stability of Au@HKUST-1, thereby laying a solid foundation for its subsequent application in gastrointestinal-related sensing studies.

3.3 Electrochemical behaviors

Electrochemical impedance spectroscopy (EIS) studies facilitate the evaluation of conductivity changes in HKUST-1 after gold incorporation. The charge transfer resistance (R_{ct}) of both HKUST-1 and Au@HKUST-1 can be calculated from EIS Nyquist plots. As shown in Fig. 3a, the composite exhibits a smaller semicircle radius than HKUST-1, indicating that Au@HKUST-1 possesses a higher charge transfer rate. Due to the efficient charge transfer process between Au and HKUST-1, the value of R_{ct} reduced by 30%. This result demonstrates that the introduction of Au enhances the electrochemical activity of the host material, contributing to improved sensitivity in electrochemical sensors.

3.4 Optimization and characterization of the fabricated electrochemical sensor

To evaluate the ability of Au@HKUST-1 toward recognizing the DA and UA, Au@HKUST-1/GCE and HKUST-1/GCE were used as working electrodes for the detection of DA (150 μM), UA (150 μM) and Mix (with 150 μM of DA and UA) in PBS solution by differential pulse voltammetry (DPV). Fig. 3b shows the significantly peak current response for Au@HKUST-1/GCE, although HKUST-1/GCE also exhibits similar response curves in 150 μM DA solution.

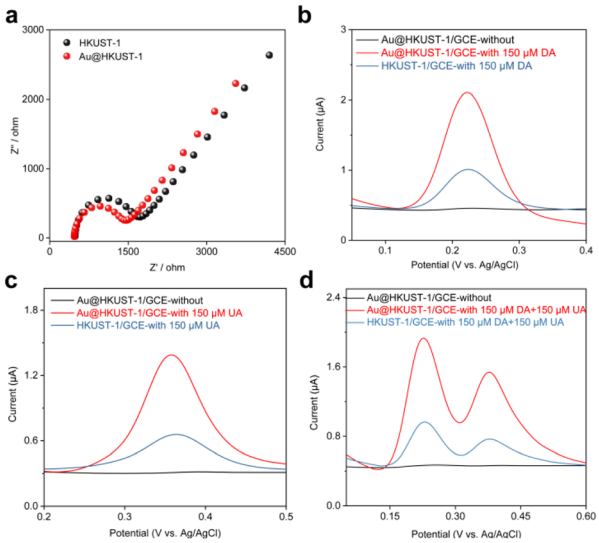

Fig. 3 (a) EIS spectra for Au@HKUST-1/GCE and HKUST-1/GCE, (b) and (c) DPV curves of Au@HKUST-1/GCE and HKUST-1/GCE in 0.1 M PBS containing 150 μM DA and 150 μM UA, respectively. (d) DPV curves of Au@HKUST-1/GCE and HKUST-1/GCE in 0.1 M PBS containing 150 μM DA and 150 μM UA.

However, the response current intensity exhibited by Au@HKUST-1/GCE is 2.2 times that of HKUST-1/GCE. In a solution without substrate, Au@HKUST-1/GCE exhibits no response current curve. This result indicated that Au and HKUST-1 play a cooperative role through intermolecular interactions. As shown in Fig. 3c and d, Au@HKUST-1/GCE shows the same trend in both UA and Mix solutions. It is worth noting that the sensor displayed the oxidation peak position attributed to UA differs from the oxidation peak position attributed to DA by about 0.15 V in the mixed solution, which could be easily distinguished from the mix of UA and LD. The effect of the PBS solution pH on the sensing performances of DA or UA on Au@HKUST-1/GCE was conducted with DPV. The response curves increased with the pH values from 5 to 7, and then increased with the pH values from 7 to 9. Due to reaching the highest response current at pH 7, we chose a PBS of pH = 7 as the support electrolyte.

Under optimized experimental conditions, we performed recognition of different concentrations of DA and UA (5–250 μM) by DPV analysis method to evaluate the performance of sensors. As shown in Fig. 4a and b, the response current continued to increase with elevated concentrations of DA. And there is a good linear relationship between the response current (I_{DA}) and concentrations of DA (C_{DA}) in the range of 5–250 μM. The linear regression equation is I_{DA} (μA) = 0.01185 C_{DA} (μM) −0.01303. The limit of detection (LOD) was calculated to be 0.06 μM according to the equation. Likewise, the Au@HKUST-1/GCE exhibited a greater oxidation current for elevated concentrations of UA in the range of 5–250 μM (Fig. 4c and d). The linear regression equations describing the relationship between changes in the response current (I_{UA}) and the concentration concentrations of UA (C_{UA}) isomers are I_{UA} = 0.00702 C_{UA} −0.00050. The limit of detection (LOD) was calculated to be 0.38 μM according to the equation. The electrochemical sensing performance of DA and UA was compared with that of other reported sensors, which can be seen that the Au@HKUST-1/GCE sensor still exhibits excellent performance. As shown in Fig. 4e and f, the synchronous response of the Au@HKUST-1/GCE sensor to UA and DA in different concentrations (C_{DA} : C_{UA} = 1 : 1). The response currents of LD and UA oxidation peaks both increase with increasing concentrations of LD and UA. The good linear relationship between I and C, which could be fitted of I_{DA} (μA) = 0.00821 C_{DA} (μM) −0.03506 for detecting DA and I_{UA} = 0.00503 C_{UA} −0.03286 for detecting UA. Therefore, the LODs of DA and UA were calculated to be 0.10 μM and 0.15 μM, respectively. Au@HKUST-1/GCE sensor can detect both UA and LD with high sensitivity and low LOD (Table S1). At the same time, this excellent LOD is also lower than the concentration of DA in the body fluids of elderly dementia patients and the concentration of UA in the body fluids of hyperuricemia patients when taking medication. The sensor has a guiding role in the health diagnosis, treatment, and medication of these patients.

3.5 Anti-interference and stability

When considering subsequent applications in digestive tract secretions, attention is typically required to ensure that the

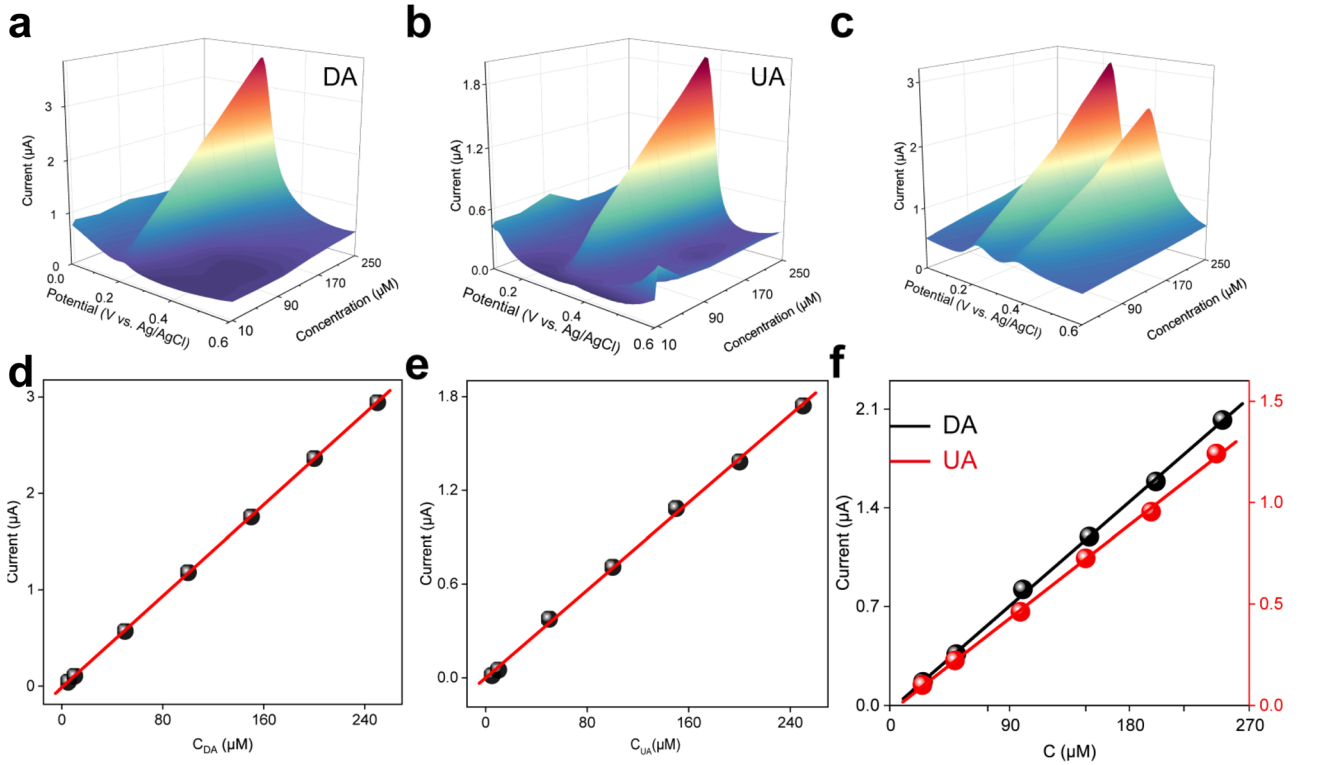

Fig. 4 DPV curves of Au@HKUST-1/GCE upon successive addition of different concentration of DA (a) or UA (b), respectively. The corresponding calibration plots of the response current *vs.* the concentration of DA (d) or UA (e), respectively. DPV curves of Au@HKUST-1/GCE upon successive addition of differentconcentration of DA and UA (c). The corresponding calibration plots of the response current *vs.* the concentration of DA and UA (f).

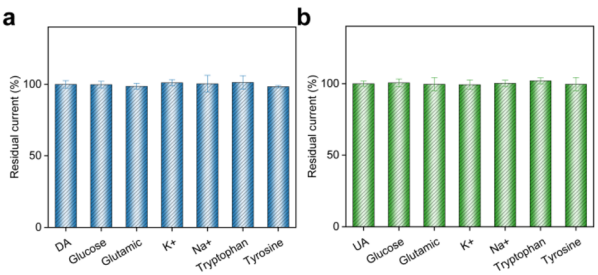

Fig. 5 Selectivity of the DA (a) and UA (b) sensor to DA and UA over common interfering species in saliva. The levels of those analytes are 100 μM DA, 100 μM UA, 50 μM glucose, 50 μM glutamic, 50 μM ascorbic acid, 50 mM Na^+, 10 mM K^+, 50 μM tryptophan, and 50 μM tyrosine.

sensor is resistant to interference. Therefore, we evaluated the impact of common saliva interferents, including Na^+, K^+, tryptophan, tyrosine, glucose, glutamate, and ascorbic acid on the detection of DA or UA by adding these substances to simulated assay solutions. The results indicate that the presence of these interferents does not affect the determination of UA and DA (Fig. 5). This demonstrates that Au@HKUST-1/GCE possesses excellent interference resistance. Therefore, Au@HKUST-1/GCE shows promise for the accurate measurement of UA and DA in gastrointestinal secretions, providing a new option for biosensor applications in health monitoring.

3.6 Analysis for real sample

To evaluate the performance of Au@HKUST-1/GCE in actual gastrointestinal secretions, quantitative amounts of DA and UA were added to artificial saliva using the standard addition method. The recovery rates of DA and UA for Au@HKUST-1/GCE were found to be between 95.5% to 103.3% and between 98.5% to 102.1%, respectively (Table S2), with relative standard deviations (RSD) of less than 4%. These results suggest that Au@HKUST-1/GCE can be successfully used to determine DA and UA in real samples.

4 Conclusion

In summary, we have developed a composite material preparation method based on HKUST-1 encapsulated Au^0 and fabricated it into an electrochemical sensor for detecting the levels of DA and UA. By modifying Au@HKUST-1 on the surface of GCE electrode, rapid and accurate detection and simultaneous monitoring of DA and UA were achieved. Electrochemical testing shows that Au@HKUST-1/GCE exhibits excellent detection performance and anti-interference ability. The excellent detection performance is attributed to the weak intermolecular interactions. Meanwhile, Au@HKUST-1/GCE exhibits good recovery rates in artificial saliva. These results contribute to precise monitoring of gastrointestinal status and health management of gastrointestinal diseases.

Author contributions

Juanjuan Ji: conceptualization, writing – original draft, writing – review & editing, data analysis, supervision. Baohong Shen: literature search and organization, data analysis, writing – original draft. Fang Yang: characterization (material and structural analysis). Sujuan Li: writing – review & editing, data analysis. Yuyu Wang: literature review, writing – original draft. Lu Yang: characterization (spectroscopic and microscopic analysis), figure preparation. Hao Lin: experimental work (sample preparation and reaction procedures).

Conflicts of interest

The authors declare that they have no known competing financial interests or personal relationships that could have appeared to influence the work reported in this paper.

Data availability

All the data supporting this article have been included in the main text and the supplementary information (SI). Supplementary information is available. See DOI: https://doi.org/10.1039/d6ra01510g.

Notes and references

1 C. Steiger, A. Abramson, P. Nadeau, A. P. Chandrakasan, R. Langer and G. Traverso, *Nat. Rev. Mater.*, 2019, **4**, 83–98.
2 J. Min, H. Ahn, H. Lukas, X. Ma, R. Bhansali, S.-H. Sunwoo, C. Wang, Y. Xu, D. R. Yao, G. Kim, Z. Li, T. K. Hsiai, A. Emami, H.-T. Jung and W. Gao, *Nat. Electron.*, 2025, **8**, 844–855.
3 G. McCallum and C. Tropini, *Nat. Rev. Microbiol.*, 2024, **22**, 105–118.
4 S. Gao, L. Yan, R. Wang, J. Li, J. Yong, X. Zhou, Y. Wei, X. Wu, X. Wang, X. Fan, J. Yan, X. Zhi, Y. Gao, H. Guo, X. Jin, W. Wang, Y. Mao, F. Wang, L. Wen, W. Fu, H. Ge, J. Qiao and F. Tang, *Nat. Cell Biol.*, 2018, **20**, 721–734.
5 C. Li, W. Yu, P. Wu and X. D. Chen, *Trends Food Sci. Technol.*, 2020, **96**, 114–126.
6 G. A. Moser and M. S. McLachlan, *Environ. Sci. Technol.*, 2002, **36**, 3318–3325.
7 X. Yin, B. Lee, J. Zaragoza and M. L. Marco, *Sci. Rep.*, 2017, **7**, 7267.
8 U. Kamran, A. Abbasi, N. Umar, I. Tahir, M. J. Brookes, M. Rutter, M. McCord, N. J. Adderley, J. Dretzke and N. Trudgill, *Endosc. Int. Open*, 2023, **11**, E835–E848.
9 W. Liu, T. Wang, M. Zhu and G. Jin, *Nutrients*, 2023, **15**, 1344.
10 M. Parolini, C. Ferrario, B. De Felice, S. Gazzotti, F. Bonasoro, M. D. Candia Carnevali, M. A. Ortenzi and M. Sugni, *J. Hazard. Mater.*, 2020, **398**, 122848.
11 S. Wei, S. Li, H. Xiao, F. Zhao, J. Zhu, Z. Chen and L. Cao, *Nanoscale Adv.*, 2023, **5**, 133–141.
12 S. S. da Silva, T. L. Valério, B. M. Hryniewicz, H. Jaradat, M. D. S. W. Araújo, C. A. Royer, B. B. Ortiz, A. E. Deller, L. Y. Kashiwagui, P. d. S. F. Guimarães, J. d. C. Oliveira, D. F. Gradia, O. Kanoun, C. C. de Oliveira and M. Vidotti, *Sens. Actuators, B*, 2025, **442**, 138136.
13 Y. Zhu, J. Xie, X. Chen and Y. Yang, *Microchem. J.*, 2026, **221**, 116841.
14 J. Salapa, A. Bushman, K. Lowe and J. Irudayaraj, *Nano Converg.*, 2020, **7**, 38.
15 Z. Nian, M. Deng, L. Ye, X. Tong, Y. Xu, Y. Xu, R. Chen, Y. Wang, F. Mao, C. Xu, R. Lu, Y. Mao, H. Xu, X. Shen, X. Xue and G. Guo, *Pharmacol. Res.*, 2024, **206**, 107280.
16 Z. Yan, Z. Shi, Y. Wu, J. Lv, P. Deng, G. Liu, Z. An, Z. Che, Y. Lu, J. Shan and Q. Liu, *Biosens. Bioelectron.*, 2023, **234**, 115363.
17 T. Ajiri, M. Zhang, N. Mizukami, M. Iida, S. Kawaguchi, Y. Sekihara, K. Chattrairat, Z. Zhu, Y. Baba, H. Koga and T. Yasui, *Biosens. Bioelectron.*, 2026, **299**, 118436.
18 Z. Li, F. Chen, N. Zhu, L. Zhang and Z. Xie, *ACS Nano*, 2023, **17**, 21935–21946.
19 X. Zhao, X. Chen, Y. Lu, Z. Zhou, P. Lin, Y. Lin, S. Hu and L. Cui, *J. Transl. Med.*, 2025, **23**, 582.
20 H. Dong, J. Zhang, T. Liu, X. Li, X. Yuan, A. He, Q. Li, Y. Zhang, W. Xiu, Z. Chu, Y. Mou and W. Jin, *Adv. Healthcare Mater.*, 2025, **14**, 2404558.
21 Y. Bi, M. Sun, J. Wang, Z. Zhu, J. Bai, M. Y. Emran, A. Kotb, X. Bo and M. Zhou, *Anal. Chem.*, 2023, **95**, 6690–6699.
22 L. Feng, K.-Y. Wang, G. S. Day, M. R. Ryder and H.-C. Zhou, *Chem. Rev.*, 2020, **120**, 13087–13133.
23 L. Vilà-Nadal and L. Cronin, *Nat. Rev. Mater.*, 2017, **2**, 17054.
24 L. Zhu, X.-Q. Liu, H.-L. Jiang and L.-B. Sun, *Chem. Rev.*, 2017, **117**, 8129–8176.
25 D. Probst, K. Batchu, J. R. Younce and K. Sode, *ACS Sens.*, 2024, **9**, 3828–3839.
26 L.-C. Tai, T. S. Liaw, Y. Lin, H. Y. Y. Nyein, M. Bariya, W. Ji, M. Hettick, C. Zhao, J. Zhao, L. Hou, Z. Yuan, Z. Fan and A. Javey, *Nano Lett.*, 2019, **19**, 6346–6351.
27 X. Xing, B. Yao, Q. Wu, R. Zhang, L. Yao, J. Xu, G. Gao and W. Chen, *Biosens. Bioelectron.*, 2022, **198**, 113804.
28 S. Ding, S. Tang and J. Wang, *Device*, 2025, **3**(7), DOI: 10.1016/j.device.2025.100782.
29 Y. Zhang, H. Yu, S. Chai, X. Chai, L. Wang, W.-C. Geng, J.-J. Li, Y.-X. Yue, D.-S. Guo and Y. Wang, *Adv. Sci.*, 2022, **9**, 2104463.
30 Y.-B. Cheng and Y. Li, *Hypertension*, 2018, **71**, 66–67.
31 L. Arabuli, P. Lovecka, R. Jezek, J. Viktorova, T. Macek, P. Junkova, R. Gakhokidze, F. Sharifianjazi, A. Esmaeilkhanian, P. Salahshour, P. Poursafa and P. Sabouri, *J. Mol. Struct.*, 2023, **1287**, 135665.
32 Y. Chen, X. Mu, E. Lester and T. Wu, *Prog. Nat. Sci. Mater. Int.*, 2018, **28**, 584–589.
33 V. Thamke, S. Suryawanshi, C. Aware, P. Mali, B. Shinde, D. Patil, M. Rane, A. Chaudhari, S. Tapase and J. Jadhav, *3 Biotech*, 2024, **14**, 126.